16th Australasian Fluid Mechanics Conference
Crown Plaza, Gold Coast, Australia
2-7 December 2007

A Force Balance to Measure the Total Drag of Biofilms on Test Plates

A. F. Barton [1], J. E. Sargison [2], P. Brandner [3], G. J. Walker [2]

[1] GWMWater
Water Resources Division, Horsham, Victoria, 3402 AUSTRALIA
[2] University of Tasmania
School of Engineering, Hobart, Tasmania, 7001 AUSTRALIA
[3]Australian Maritime College
Launceston, Tasmania, 7250 AUSTRALIA

Abstract

A floating force balance has been designed and integrated into the working section of a recirculating water tunnel to enable the measurement of total drag on test plates, which form part of the tunnel wall.

Measurements completed include a calibration of the rig using a smooth acrylic plate, a smooth painted plate, and an artificially roughened plate. The painted plate and rough plate have also been studied with biofilms attached to their surface. The water tunnel and total drag rig have been built specifically to allow the detailed investigation of freshwater biofilm effects have on the flow through hydraulic conduits.

Calibration results show that useful information can be obtained by using the force balance, particularly in association with other measurement techniques. Research into the effects of biofilms showsthat large increases in friction and effective roughness can be expected.

Introduction

As part of a biofouling research program at the University of Tasmania, a purpose built water tunnel was constructed to enable the detailed measurement of the skin friction properties of various surfaces, including low friction paints and surfaces covered with biofilms.

In addition to measuring skin friction character by boundary layer traverses, a total drag rig was designed and incorporated into the working section of the water tunnel.

This paper presents a brief overview of the water tunnel facility, details of the working section, and describes the associated instrumentation including the load cell used to conduct total drag measurements on a section of the wall. Results presented include general flow conditions of the working section and calibration results of the drag rig, including estimates of error. Results are then presented for smooth and rough test plates, both clean and with biofilms attached. A brief discussion of the work is provided along with conclusions.

Water Tunnel and Working Section

A closed loop, recirculating water tunnel was built specifically for the controlled and detailed measurement of local skin friction and drag, and general boundary layer research. The design of the facility, shown schematically in Figure 1, was based on wind tunnels used in aeronautical research. A number of components were specially designed to encourage controlled and uniform flow conditions within the working section. The bulk flow speed through the working section of the tunnel ranges from 0.3 m/s to over 2 m/s, and may be controlled via computer to maintain a constant Reynolds number for the duration of any measurement.

Further information on the design and calibration of the water tunnel can be found in [1].

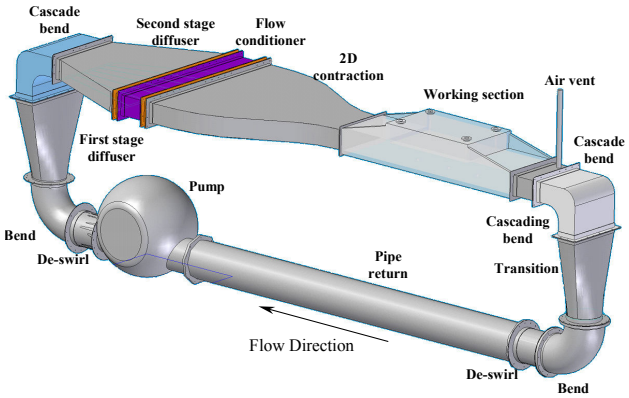

Figure 1: The water tunnel used for measuring total drag on test plates.

The working section forms the measurement centre of the water tunnel where test plates are mounted for study. Figure 2 shows the working section, constructed entirely of 30 mm thick acrylic sheeting, and measuring 2200 mm long, 200 mm high, and 600 mm wide. During water tunnel operation, the entire test surface, force balance rig and roof cavity is flooded with water. The test surface was fabricated from stainless steel plates measuring 997mm long by 597 mm wide by 3 mm thick, or an acrylic plate of the same area but 5 mm thick. These plate dimensions provided a nominal 1.5 mm clearance around the edges of the test plate, which was required to ensure that the force balance was floating. These clearances were based on practical requirements for balance assembly and disassembly.

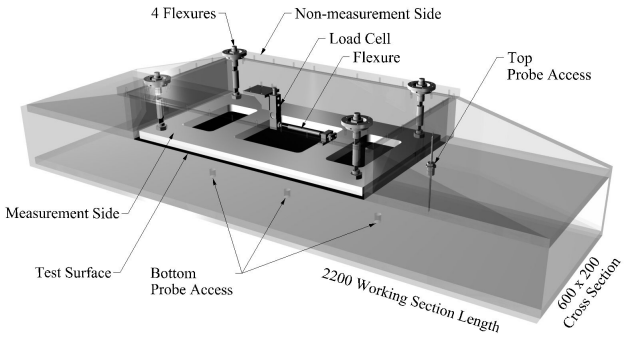

Figure 2: Diagram of working section with the various components labelled.

A strain-gauge force balance arrangement was used for the total drag measurements. The test plate was suspended from the lid of the working section by four precision-machined stainless steel flexures. An MTI Weigh Systems single ended shear beam load cell (model MTI-4856-SB) was attached to the lid of the working section and connected via a load transfer rod to the acrylic backing of the test plate. The flexures ensured a one-dimensional transfer of force through the load transfer rod to the load cell, which was connected to a Mann Industries strain gauge transmitter and personal computer for data acquisition using LabView software.

Flow Characteristics of the Working Section

It was important to know the condition of the flow through the working section to ensure the most appropriate treatment of data obtained from any drag measurement.

Winter [2] describes some of the problems associated with direct drag measurement using floating force balances. Problems of particular note for the present study, which have been considered, are flow leakage around the edges of the test plate; the provision of a transducer for measuring small forces, and the compromise between the requirement to measure local properties and the necessity of having a measurement element of sufficient size that the force on it can be measured accurately. The effects of misalignment of the floating element test plate, and the effects of temperature changes are also important in the system set up and analysis of measurements. The last two problems are discussed more in the calibration section of this paper.

The design of a floating force balance necessarily requires clearances around the test plate edges and this gives rise to particular flow characteristics of interest. The pressure in the cavity above the test plate was an average of the static pressure over the plate, and hence there was leakage of flow from mainstream into the cavity at the leading edge and leakage from the cavity back into the flow at the trailing edge of the plate.

This was of greatest consequence at the leading edge of the test surface. Figure 3 shows the effects of flow leakage with the use of boundary layer shape factors. The drop in shape factor, H shows the discontinuity in boundary layer as water flows over the gap at leading edge of test plate. Boundary layer measurements clearly show a developing mean velocity profile, which is interrupted at the leading edge of the test plate due to the gap required for total drag measurements. Data for the boundary layer shape factor under equilibrium conditions are also shown in the Figure for comparison.

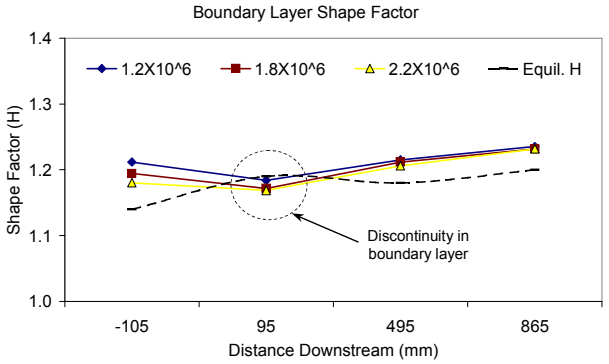

Figure 3: Plot of boundary layer shape factors showing development of boundary layer over the length of the test plate surface. Data are shown for three different Reynolds numbers based on test plate length.

The working section was measured to have a slightly non-uniform vertical velocity profile, shown in Figure 4. This is thought to be due to secondary flows causing accumulation of low energy fluid on the inside circumference of the water tunnel bends.

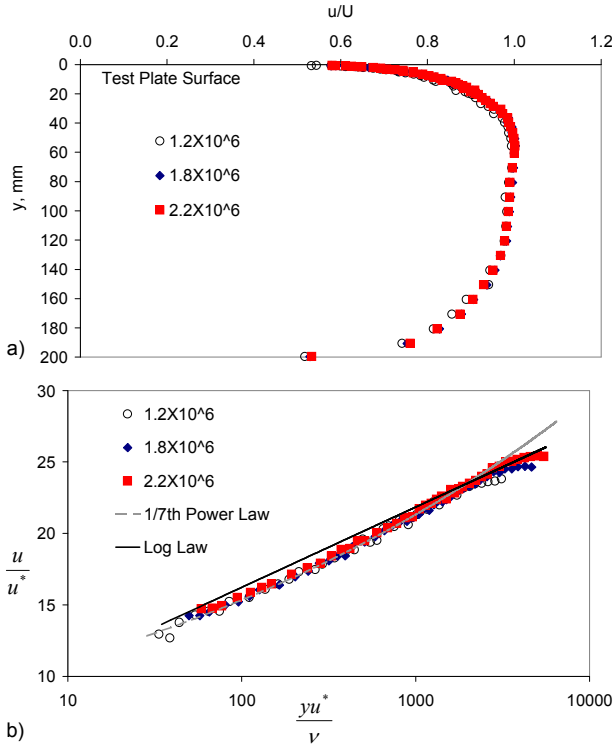

Figure 4: Vertical mean velocity profile (a) and boundary layer mean velocity profile (b) in the working section, measured 865mm downstream of the leading edge of the test plate. Data are shown for three different Reynolds numbers based on test plate length.

In addition to this, evidence of secondary flows was observed within the working section. Figure 5 shows the static pressure variation measured across the test plate surface at the approximate mid section which indicates evidence of longitudinal vortices in the corners. The edge effects are due to both longitudinal corner vortices and the movement of water between the edges of the test plate and the roof cavity in the working section (flow leakage). However, these are confined to regions within 50mm of the sidewall.

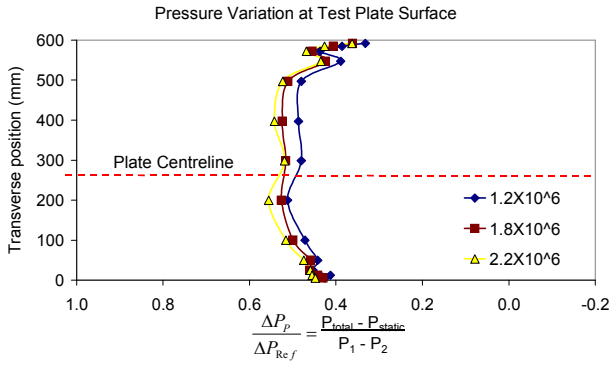

Figure 5: Pressure variation at the test plate surface measured at the approximate halfway length. Data are shown for three Reynolds numbers based on test plate length.

Boundary Layer Development

The appropriate treatment of the turbulent boundary layer development was important in the present study, as the boundary layer thickness was not known prior to any of the total drag measurements. All of the equations used depended on knowing the state of the boundary layer at the leading edge of the test surface for accurate estimates of drag and associated estimates of roughness.

Both the log law and the 1/7th power law approximate the velocity distribution in a fully turbulent boundary layer shown in Figure 4 and [1]. The boundary layer thickness, δ, was derived from the momentum thickness using θ = 7/72(δ) as given by the 1/7th power law. The boundary layer momentum thickness is a more reliable parameter in the present situation as it is less sensitive to error in determining the wall position.

The drag coefficients of a flat plate of width b and length l in a stream of velocity U and density ρ is defined by Equation 1 [3].

$$Drag_{(Plate)} = C_{D_{Plate}} \rho b l_{Plate} \frac{U^2}{2} \qquad 1$$

To compare experimental results for plate drag with theoretical models for an isolated plate it is first necessary to allow for the initial non-zero boundary layer thickness at the leading edge of that test plate.

This was done by estimating a virtual origin at distance l_1 upstream from which a continuously turbulent boundary layer on an isolated plate would produce the same initial boundary layer thickness. Figure 6 shows the concept of the virtual origin of the turbulent boundary layer, and the definitions for Equations 1, 2 and 3.

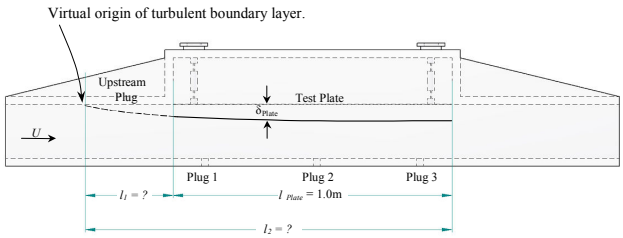

Figure 6: Assumed boundary layer development over the test surface.

For a smooth flat plate, with known boundary layer thicknesses at measurement positions, plug 1, 2 and 3 (from mean velocity boundary layer traverses), the value of l_1 was found by using Equations 2 and 3 [3] based on the 1/7th power law for the turbulent boundary layer velocity distribution.

$$l_1 = \frac{\delta \mathrm{Re}_{l_1}^{0.167}}{0.22} \qquad 2$$

Note that δ was derived from the boundary layer momentum thickness. Equation 3 can be applied for hydraulically smooth conditions.

$$C_D = \frac{0.074}{\mathrm{Re}_l^{\frac{1}{5}}} \qquad 3$$

Re_l is the Reynolds number based on the length of l. Typical values of Re_l for the acrylic calibration plate used in the present study ranged from 8.3×10^5 to 3.2×10^6 for $l_1 = 1.39$m.

The theoretical drag for the test plate was then obtained from Equation 4.

$$Drag_{(Plate)} = C_{D(l_2)} \rho b l_2 \frac{U^2}{2} - C_{D(l_1)} \rho b l_1 \frac{U^2}{2} \qquad 4$$

Where the equivalent sandgrain roughness, k_s, was of interest, Equation 5 was used to find C_D, as suggested by [3]. The distance, l, was the equivalent upstream length, the plate length, or both. An iterative method was used to find k_s, which was incrementally adjusted until values matched for both $C_{D(l_1)}$ and $C_{D(l_2)}$.

$$C_D = \left(1.89 + 1.62 \log \frac{l}{k_s}\right)^{-2.5} \qquad 5$$

Drag Rig Calibration

To calibrate the load cell for total drag measurements, the whole arrangement is removed from the tunnel supplementary volume and placed on a test jig allowing precise alignment of measurement side and calibration forces. The lid and plate were adjusted to be parallel with each other and to be horizontal. Forces were applied in 0.49 N (using 50 gram masses) increments. Changes in volts due to the applied force were recorded to personal computer via LabView software. Accuracy for the masses used for calibration was 0.4%.

Figure 7 shows a typical calibration for the drag rig. A new calibration was completed every time a new plate was required for measurement in the water tunnel. For example, the acrylic calibration plate, which was 5mm thick (stainless steel plates were 3mm thick), required a small height adjustment in the flexures to ensure the plate was flat and aligned with the working section roof. This resulted in a slight angle change in the load transfer rod, and thus a re-calibration was required. When the thinner steel plates were subsequently used, the rig was then recalibrated.

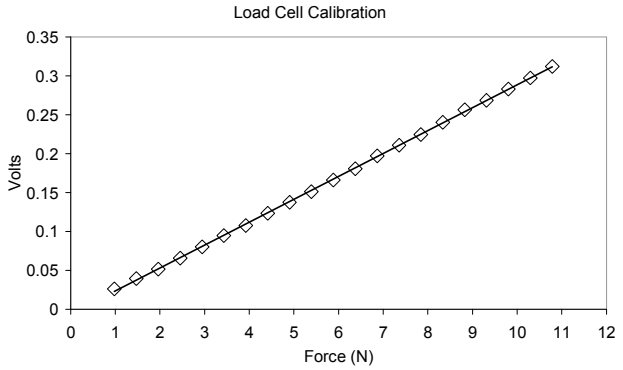

Figure 7: Typical drag rig calibration plot showing the measured voltage output for given loads.

An estimate of error in the measured drag was made using the RMS of the deviations of the calibration curve in Figure 7. This error plot is shown in Figure 8. An error in voltage at these RMS values was propagated though the data reduction procedure, and an uncertainty of ± 2.7 % (with confidence 95%) in C_D was found.

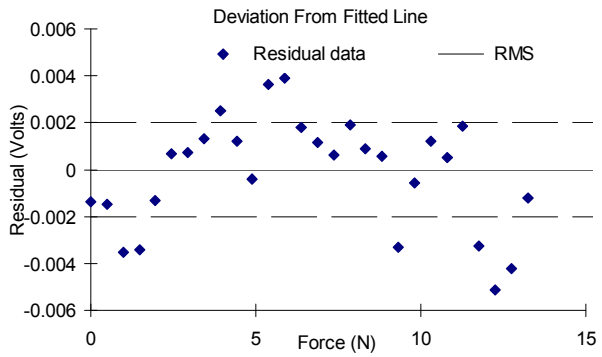

Figure 8: Error estimates of drag rig from calibration with known forces.

An additional correction was applied to the drag data due to the forces arising from the development and growth of the boundary layer through the working section and resulting streamwise bulk flow acceleration and associated pressure gradient.

The correction was made by measuring the pressure difference between the ends of the plate (using static wall tappings), and multiplying this pressure across the test plate end cross sectional area. The net pressure force on the ends of the plate was then subtracted from each drag measurement. The stainless steel test plate end sectional area of 0.001791 m^2 gave typical force corrections of approximately 0.3 N. This equated to a maximum of approximately 10 % of measured drag for clean smooth plates and approximately 2.5 % of measured drag for biofouled plates for the results shown in Figures 10 and 12.

After some initial calibration tests of the ability of the drag rig to accurately measure the drag of an acrylic calibration plate, it was found the temperature changes to the water and ambient air were able to significantly influence drag measurements. Even modest changes in temperature were able to cause significant drifts in drag measurements due to thermal strain (expansion and contraction) of the rig with associated forces being transferred to the load cell. This was overcome by measuring a zero drag (i.e. no flow) with each drag measurement. The zero was then subtracted from the measured drag to remove any drift problem.

However, the largest source of error in measured drag was uncertainty associated with errors in plate alignment and the variation of clearances around the plate.

A repeatability test was performed using an acrylic calibration test plate to better find the typical deviation of measured drag from the mean. To do this, drag measurements were made 10 times at three flow Reynolds numbers (30 drag measurements in total). Small changes in the plate alignment were made by randomly varying the gap widths around the edge of the plate. The RMS of the deviations was found to be ±0.0108 volts (Figure 6), which is considerably larger than the ±0.0020 volts of the calibration curve in Figure 8. This also implies greater uncertainty with reducing flow velocity and Reynolds numbers and explains the greater variability in C_D at lower Reynolds numbers for drag measurements presented in Figures 10 and 12. Figure 9 incorporates all possible error scenarios including changes in plate alignment, corrections due to pressure forces, and corrections due to temperature effects. Error bars presented in Figure 10 and 12 reflect the error estimates shown in Figure 9.

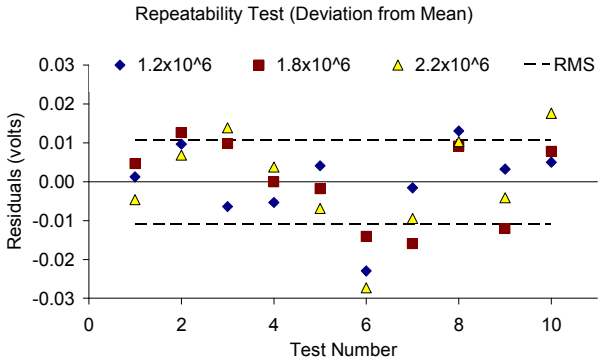

Figure 9: Error results for the repeatability test at three different Reynolds numbers (based on test plate length).

Results

The first set of results presented in Figure 10 show total drag measurements for a clean smooth painted plate and a clean artificially roughened plate. The drag measurements were conducted at intervals in pump speed and associated plate Reynolds numbers. The total drag force on the plate was measured as a voltage output from the strain gauge signal conditioner and acquired by computer using the LabView software as described earlier. The voltage was then converted to a force (N) using the bench top calibration data.

To optimise measurement precision of the total drag coefficient (due to friction), C_D, on the plate, and to satisfy the problems listed by Winter [2], it was important in the first instance to correctly align the plate in the water tunnel. The test plate dimensions allowed for a design gap of 1.5 mm on each side of the plate in the working section. The actual gap varied from 1 mm to 2 mm on the various edges of the plate due to practical difficulty in alignment and tolerance associated with the construction of the equipment.

Data in Figures 10 and 12 are presented with the theoretical values of a hydraulically smooth test plate for comparison. The smooth plate data compares very well to the theoretical smooth plate data. Other test plates tested in the present research include a plate artificially roughened with sand grains, and smooth and roughened plates covered with biofouling. The drag data for the rough plate also shows good results, as the equivalent sandgrain data (k_s = 2.09 mm ± 0.49mm) derived from the drag measurements compare well to the particle size distribution

shown in Figure 11. Other results from [1, 4-6] also show good comparison between theoretical values and measured data. The results indicate that adequate corrections have been made to the data to enable a meaningful analysis of results.

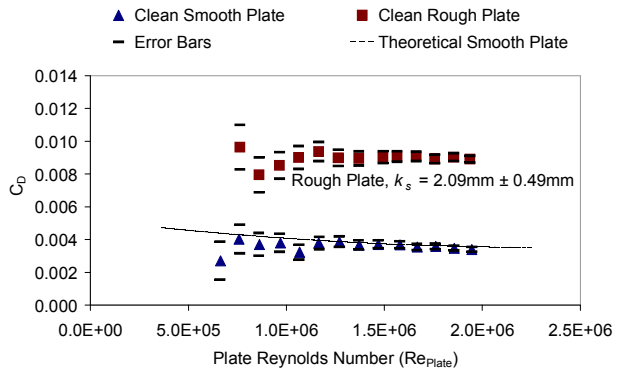

Figure 10: Total drag results for clean test plates.

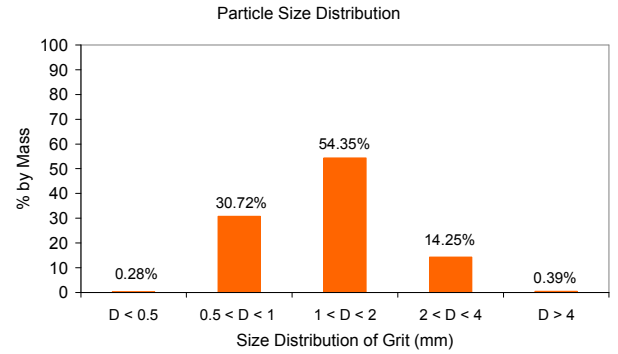

Figure 11: Particle size distribution for grit used to artificially roughen the test plate.

Figure 12 presents data taken from the smooth painted plate and artificially roughened plate with biofilms attached to their surface. Both test plates were deployed in an open channel system for several months and allowed to have a low-form, gelatinous biofilm develop on their respective surfaces. The flow through the open channel where the plates were deployed had a bulk flow speed of approximately 0.5m/s-1m/s, and so the biofilms were already pre-conditioned to moving water prior to placement in the water tunnel for testing.

The results show that the biofilm has significantly roughened the smooth plate, which now has an equivalent roughness, k_s = 1.90mm ± 0.26mm. The rough plate has also increased its roughness to k_s = 3.10mm ± 0.72mm.

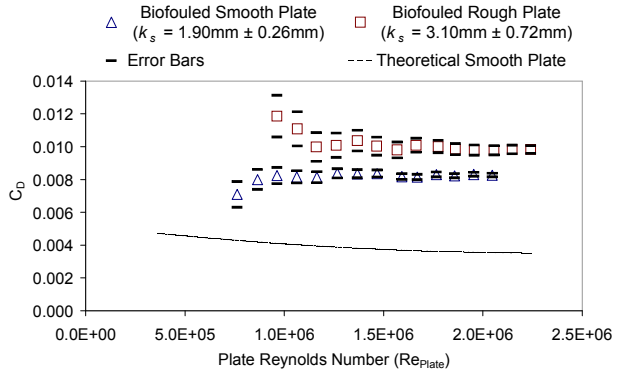

Figure 12: Total drag results for biofouled test plates.

Although the test plates have both been significantly roughened by biofouling material, it is the smooth plate that has had the greatest relative increase in measured drag from its clean condition. This could have serious economic consequences if appropriate low-friction and anti-fouling paints are not used in hydraulic conduits such as found in hydroelectric systems. Deterioration of hydraulic efficiency due to biofouling is a significant issue for many hydroelectric and other water authorities [7-11].

Discussion

Results presented in this paper show that the force balance used to undertake total drag measurements is useful for measuring the influence of roughness properties of various surfaces on skin friction and drag.

Boundary layer measurements within the working section clearly show a developing mean velocity profile (Figure 3), which is interrupted at the leading edge of the test plate due to the gap required for total drag measurements. Both the log law and the $1/7^{th}$ power law approximate the velocity distribution.

It is also noted that the water tunnel may be producing a slightly non-uniform velocity distribution in the vertical direction (Figure 4). To help counter the resulting uncertainties in determining the total boundary layer thickness, the momentum boundary layer thickness was used to estimate the boundary layer thickness, with the additional advantage of this value not being as sensitive to an accurate wall position as other methods.

Edge effects were observed due to longitudinal corner vortices and the movement of water between the edges of the test plate and the roof cavity in the working section. However, these are confined to regions within 50mm of the sidewall (Figure 5) and a good understanding of these effects has allowed appropriate consideration to be made with regard to the treatment of results.

The total drag measurements, while not exactly replicating theoretical values, display the general characteristics required to gain useful information. The drag measurements are affected by the leakage of flow into the roof cavity at the leading edge of the test plate, which reduces the boundary layer thickness, and increases the skin friction at the front section of the plate.

The results are more uncertain at lower Reynolds numbers where the magnitude of forces contributing towards the errors is large compared to the measured drag force at lower flow speeds. There may also be some flow unsteadiness from the pump control system used to maintain constant Reynolds number flows.

Results of the biofouled test plates show significant increases in drag compared to the respective clean plate conditions. This fact is of considerable concern in hydroelectric and other water authorities who depend on the hydraulic efficiency of hydraulic conduits for economic reasons. The University of Tasmania is engaged in several areas of biofouling research, including low friction surfaces, environmentally friendly biocides and anti-fouling paints, and better understanding the mechanisms by which biofilms dissipate energy in the near wall flow environment.

Conclusions

This paper has described a total drag balance, incorporated into the wall of a newly constructed water tunnel, and shown that the instrument is useful for the measurement of total drag and associated roughness for a number of test surfaces.

The total drag balance is particularly useful when used in conjunction with boundary layer traverses, which also gives information on local skin friction and roughness properties.

The water tunnel has been successfully used to measure the friction, roughness and boundary layer characteristics of freshwater biofilms found in hydraulic conduits. Investigations continue at the University of Tasmania into the properties of biofilms and their effects of flow, and also the friction properties of paints and other materials.

Acknowledgments
Hydro Tasmania and the Australian Research Council under the Linkage Grants Scheme provided financial support for this project. The author also acknowledges e-Water CRC and GWMWater for support in paper preparation and conference attendance.

List of Notation
b = test plate width
C_D = Coefficient of total drag
H = Boundary layer shape factor = δ^*/θ
k_s = equivalent sandgrain roughness
l = length
Re = Reynolds number
Re_l = Reynolds number based on length, l
Re_{plate} = Reynolds number based on test plate length
U = Mean velocity
u = local velocity
u^* = wall shear
y = distance from wall
δ = Boundary layer thickness
δ^* = Boundary layer displacement thickness
θ = Boundary layer momentum thickness
ν = kinematic viscosity
ρ = density

References
[1] Barton, A.F., *Friction, Roughness and Boundary Layer Characteristics of Freshwater Biofilms in Hydraulic Conduits*. 2007, PhD Thesis, University of Tasmania: Hobart, Tasmania, Australia.
[2] Winter, K.G., An outline of the techniques available for the measurement of skin friction in turbulent boundary layers. *Prog. Aerospace Sci*., 1977. 18: p. 1-57, Pergamon Press. Printed in Great Britain.
[3] Schlichting, H., *Boundary Layer Theory*. 7th Edition. 1979: McGraw-Hill.
[4] Barton, A.F., Sargison, J.E., & Walker, G.J. *Effects of Freshwater Biofilms on Flow Over Rough Surfaces*. in IAHR 6th International Symposium on Ecohydraulics. 18-23 February, Christchurch Convention Centre. 2007. Christchurch, New Zealand. CD-ROM.
[5] Osborn, J.E., Bae, Y.-S., Grenness, M.J., Sargison, J.E., Barton, A.F., Sprent, A.S., Walker, G.J., & Bendall, T. *Mapping Surface Biofilms to Improve the Efficiency of Water Conveyance*. in Spatial Sciences Congress. 2005. Melbourne: Spatial Sciences Institute of Australia, September 2005.
[6] Barton, A.F., Sargison, J.E., Walker, G.J., Osborn, J.E., & Brandner, P.A. *A baseline study of the effect of freshwater biofilms in hydraulic conduits*. in XXXI IAHR Congress. 2005. Seoul, Korea: Conference Proceedings CD ROM.
[7]. Barton, A.F., Sylvester, M.W., Sargison, J.E., Walker, G.J., & Denne, A.B. *Deterioration of Conduit Efficiency Due to Biofouling*. in 8th National Conference on Hydraulics in Water Engineering. 2004. 13-16 July, ANA Hotel Gold Coast, Queensland, Australia: Engineers Australia.
[8]. Pollard, A.L. & House, H.E., *An unusual deposit in a hydraulic tunnel*. *ASCE Journal of the Power Division*, 1959. December: p. 163-171.
[9] Minkus, A.J., *Deterioration of the hydraulic capacity of pipelines*. *New England Water Works Association*, 1954. LXVIII(1): p. 1-10.
[10] Brett, T., Head-loss Measurements on Hydroelectric conduits. *ASCE Journal of the Hydraulics Division*, 1980. 106(1): p. 173-190.
[11] Picologlou, B.F., Zelver, N., & Charaklis, W.G., Biofilm Growth and Hydraulic Performance. *ASCE Journal of the Hydraulics Division*, 1980. HY5: p. 733-747.